Biomaterials 32 (2011) 3481–3486

Contents lists available at ScienceDirect

Biomaterials

journal homepage: www.elsevier.com/locate/biomaterials

Co-encapsulation of magnetic nanoparticles and doxorubicin into biodegradable microcarriers for deep tissue targeting by vascular MRI navigation

Pierre Pouponneau [a,b], Jean-Christophe Leroux [b,c], Gilles Soulez [d], Louis Gaboury [e], Sylvain Martel [a,*]

[a] NanoRobotics Laboratory, Department of Computer and Software Engineering and Institute of Biomedical Engineering, École Polytechnique de Montréal (EPM), C.P. 6079, Succursale Centre-ville, Montréal, Québec, Canada H3C 3A7
[b] Faculty of Pharmacy, Université de Montréal, P.O. Box 6128, Dowtown Station, Montréal, Québec H3C 3J7, Canada
[c] Department of Chemistry and Applied Biosciences, Institute of Pharmaceutical Sciences, ETH Zürich, Wolfgang-Pauli-Str. 10, HCI H 301, 8093 Zürich, Switzerland
[d] Research Imaging Platform, Centre de Recherche du Centre Hospitalier de l'Université de Montréal (CRCHUM), Department of Radiology, Centre Hospitalier de l'Université de Montréal (CHUM)-Hôpital Notre-Dame, Pavillon Lachapelle, 1560 Sherbrooke Est, Montréal, Québec, H2L 4M1, Canada
[e] Département de Pathologie et de biologie cellulaire et Institut de Recherche en Immunologie et en Cancérologie (IRIC), Université de Montréal, P.O. Box 6128, Dowtown Station, Montréal, Québec H3C 3J7, Canada

ARTICLE INFO

Article history:
Received 10 December 2010
Accepted 31 December 2010
Available online 18 February 2011

Keywords:
Magnetism
Nanoparticle
Microencapsulation
MRI (magnetic resonance imaging)
Drug delivery
Liver

ABSTRACT

Magnetic tumor targeting with external magnets is a promising method to increase the delivery of cytotoxic agents to tumor cells while reducing side effects. However, this approach suffers from intrinsic limitations, such as the inability to target areas within deep tissues, due mainly to a strong decrease of the magnetic field magnitude away from the magnets. Magnetic resonance navigation (MRN) involving the endovascular steering of therapeutic magnetic microcarriers (TMMC) represents a clinically viable alternative to reach deep tissues. MRN is achieved with an upgraded magnetic resonance imaging (MRI) scanner. In this proof-of-concept preclinical study, the preparation and steering of TMMC which were designed by taking into consideration the constraints of MRN and liver chemoembolization are reported. TMMC were biodegradable microparticles loaded with iron-cobalt nanoparticles and doxorubicin (DOX). These particles displayed high saturation magnetization (Ms = 72 emu g^{-1}), MRI tracking compatibility (strong contrast on T2*-weighted images), appropriate size for the blood vessel embolization (~50 μm), and sustained release of DOX (over several days). The TMMC were successfully steered *in vitro* and *in vivo* in the rabbit model. *In vivo* targeting of the right or left liver lobes was achieved by MRN through the hepatic artery located 4 cm beneath the skin. Parameters such as flow velocity, TMMC release site in the artery, magnetic gradient and TMMC properties, affected the steering efficiency. These data illustrate the potential of MRN to improve drug targeting in deep tissues.

1. Introduction

Magnetic targeting was proposed 30 years ago as a means to increase cytotoxic agent concentration in tumors [1–4]. This approach consists in applying an external magnetic field to trap drug-loaded carriers in a targeted site [5]. Magnetic carriers, generally made with iron oxide, have been developed for the treatment of tumors located in organs such as brain [6,7], lungs [2], and liver [8,9]. Despite an increase in the amount of particles reaching the targeted area [2,6,10], such carriers are also delivered to a significant extent to healthy tissues/organs after systemic administration. This moderately controlled process may result in side effects thereby limiting the maximal tolerated dose [11]. Furthermore, since the targeting efficiency depends on the distance between the magnet and the tumor [12,13], this approach is only applicable for the treatment of superficial cancers, or tumors implanted in small animals. Indeed, the magnetic targeting of deep tissues is highly challenging [2], and is not used in clinical practice [14].

Recently, a new approach referred to as magnetic resonance navigation (MRN) has been proposed to steer and track in real time endovascular magnetic carriers in deep tissues to target areas of interest [15–18], and restrain the systemic carrier distribution. MRN is achieved with a clinical magnetic resonance imaging (MRI) scanner upgraded with an insert of steering coils [18,19]. The scanner allows tracking the carrier during MRN along a pre-planned trajectory. The magnetic field (1.5 T or higher) of the system enables saturation magnetization (Ms) of ferromagnetic materials throughout the body [15,17]. Hence, the problem of weaker magnetic field in deep tissues observed with external magnet can be

* Corresponding author. Tel.: +1 514 340 4711x5098; fax: +1 514 340 5280.
E-mail address: sylvain.martel@polymtl.ca (S. Martel).

0142-9612/$ – see front matter © 2011 Elsevier Ltd. All rights reserved.
doi:10.1016/j.biomaterials.2010.12.059

overcome. A magnetic gradient is generated to steer the carrier in a particular direction. Since a clinical MRI scanner generates a 40-mT m^{-1} gradient, only millimeter-scale carriers can be piloted [15,19]. To achieve MRN of micrometer-scale carriers for therapeutic purposes, steering coils generating a gradient up to 400-mT m^{-1} are needed [16,18,19]. Moreover, the successful application of MRN is relying on several medical [16] and MRN parameters such as magnitude of the steering magnetic gradient [18], Ms and diameter of the carrier [17], blood vessel properties (flow velocity and diameter) [16,20] and injection site position (Fig. 1A).

In this manuscript, the conception and *in vivo* steering of therapeutic magnetic microcarriers (TMMC) designed for the treatment of hepatocellular carcinoma (HCC) *via* trans-arterial chemoembolization (TACE) in the hepatic artery (Fig. 1) are reported. HCC remains the third cause of death related to cancer [21]. Improvements in current therapeutic modalities are critically required since treatment of unresectable HCC is associated with a low survival rate [22]. By controlling chemoembolic material distribution, MRN could improve embolization and drug concentration in the tumor area while limiting chemoembolization of healthy blood vessels and the hepatic complications [23–25] (Fig. 1). The TMMC characteristics such as diameter and drug release profile were based on drug eluting beads (DEB) design. DEB are recognized as promising chemoembolic systems by inducing tumor anoxia due to physical obstruction of blood flow and to the sustained release of a cytotoxic agent (*e.g.* doxorubicin, DOX) [26–29]. The TMMC consisted of biodegradable poly(D,L-lactic-*co*-glycolic acid) (PLGA) microparticles loaded with the antitumor drug and magnetic nanoparticles for steering and tracking (Fig. 1B). In this feasibility study, physiological parameters (of the rabbit) were taken into consideration for designing the TMMC. Our previously published *in vitro* data [16] indicated that the TMMC mean diameter should be 50 μm to get a distal embolization without extravasation in liver parenchyma and that the microparticles should contain 30% FeCo nanoparticles (*w/w*) to give adequate Ms for steering (Fig. 1C). FeCo nanoparticles were preferred over iron oxide nanoparticles because of their higher Ms [30] which reduces the magnetic material loading in TMMC [16].

2. Materials & methods

2.1. FeCo nanoparticles

FeCo nanoparticle synthesis, annealing and preparation for the encapsulation process are described in the supplementary information section.

2.2. Encapsulation of FeCo nanoparticles and doxorubicin

Doxorubicin-HCl (15 mg) (Sigma Aldrich, Oakville, ON, Canada) was stirred with borate buffer (pH = 8.6, 6 mL) and dichloromethane (DCM) (400 mL) (ACP, Montréal, QC, Canada). After 24 h, DCM with DOX (400 mL) was extracted from the borate buffer and stored at 4 °C. A second extraction step of 24 h was performed with DCM (400 mL). DCM with DOX (800 mL) was evaporated under rotation under vacuum until a volume of 2 mL remained. This solution was added to FeCo nanoparticles (190 mg) in DCM (1.8 mL). Under an argon flux, the volume was reduced to 2.2 mL and then added with PLGA (210 mg) (M_w = 40,000–70,000; L/G molar ratio = 50/50) (Sigma Aldrich). The mixture FeCo-DOX-PLGA-DCM (1.2 mL) was emulsified (5000 rpm, 5 min) with 1% poly(vinyl alcohol) (PVAL, 88% hydrolyzed, M_w = 13,000–23,000) (Sigma Aldrich) aqueous solution (*w/v*) (2.5 mL). Then, the emulsion was transferred to an aqueous solution of 1% PVAL (10 mL), and DCM was evaporated by rotation under vacuum during 50 min. The microparticles were washed by 4 successive centrifugation-resuspension steps (1000 × *g*, 5 min). TMMC were collected on a 20-μm filter. TMMC were sealed under argon atmosphere and stored at −20 °C until use.

2.3. Characterization experiments

FeCo nanoparticles were imaged with a transmission electron microscopy (TEM) (Jeol 2100F, Tokyo, Japan), and the chemical analysis was determined by energy dispersive spectrometry (EDS) (Inca, Oxford Instrument, Abingdon, U.K). TMMC size distribution was measured by image analysis of data obtained by optical microscopy (Imager Z1, Carl Zeiss Canada, Toronto, ON, Canada). For the fluorescence microscopy analysis, a custom filter set was added to the optical microscope. TMMC were imaged by field emission gun scanning electron microscopy (FEG-SEM) (Jeol JSM-7600TFE). FeCo nanoparticles and TMMC magnetic properties were measured with a vibrating sample magnetometer (VSM) (Walker Scientific, Worcester, MI) at room temperature. The FeCo nanoparticle loading in TMMC was determined according to Ms measurements [16]. The DOX loading was measured by spectrophotometry at 481 nm (Safire plate reader, Tecan, Durham, NC) following the dissolution of the microparticles in dimethyl sulfoxide (1.5 mL) and FeCo nanoparticle sedimentation by centrifugation (16,000 × *g*, 5 min).

2.4. In vitro steering

The MRI steering setup (Supplementary Fig. S3) is described in the supplementary information section. TMMC (3 mg) suspended in 0.9% NaCl solution (7 mL) (Baxter Corporation, Pointe-Claire, QC, Canada) were slowly injected (2.5 mL min^{-1}) with 0.027 lumen Progreat catheter (Terumo, Tokyo, Japan). The catheter tip was placed at 20 or 33 mm from the right/left bifurcation. Each steering assay was repeated at least three times. TMMC were collected at each channel outlet. To determine the steering efficiency, DOX was measured by spectrofluorimetry (λ_{ex} = 481, λ_{em} = 595) (Safire plate reader).

2.5. In vivo steering

Ten New Zealand rabbits (3.7 kg ± 0.1, Charles River, QC, Canada) were used. The study was conducted in accordance with the Canadian Council for Animal Care Guidelines and approved by the Ecole Polytechnique de Montréal and the Centre

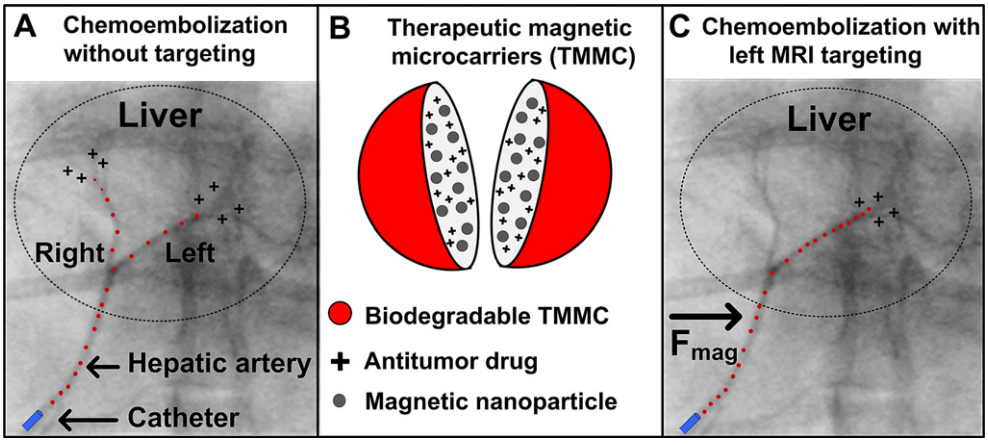

Fig. 1. Representation of MRI targeting with TMMC for liver chemoembolization. Images A and C are fluoroscopy images of the rabbit hepatic artery with superposed images of the TMMC distribution without (A) and with (C) the MRI targeting. On image A, the microparticles are released from the catheter in the artery and distributed to both lobes. Image B illustrates a schematic representation of a cut of the TMMC loaded with an antitumor drug and magnetic nanoparticles embedded into a biodegradable matrix. Image C displays the MRI targeting of the left bifurcation using the magnetic force (F_{mag}) to preserve the right lobe from the chemoembolization.

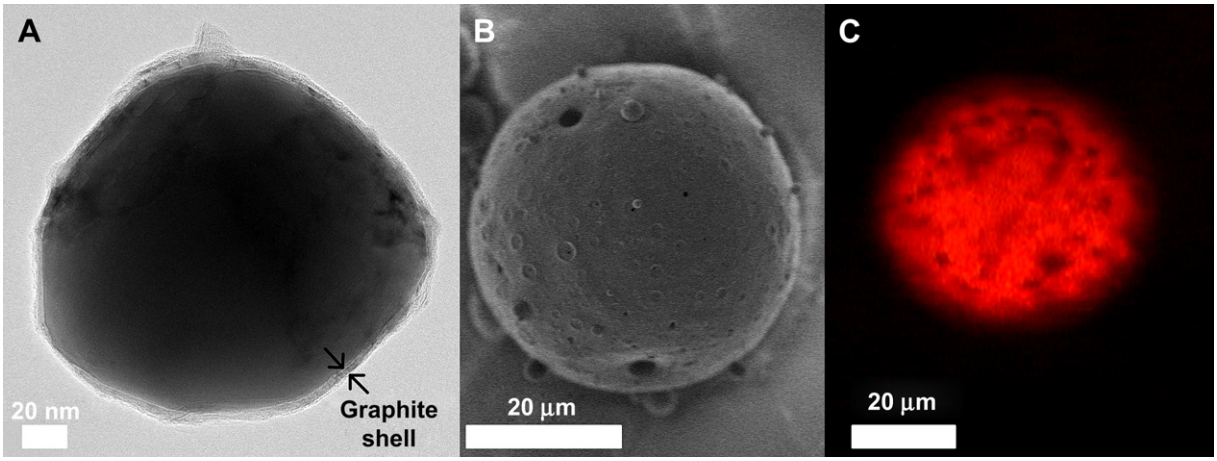

Fig. 2. A) TEM image of a FeCo nanoparticle coated with a graphite shell. B) SEM image of a TMMC exhibiting apparent porosity. C) Fluorescence microscopy image of a TMMC. The fluorescence signal comes from the encapsulated DOX.

Hospitalier Universitaire de Montréal (CHUM) animal care committees. Four rabbits received an injection of TMMC with an MRI steering, three rabbits received a TMMC injection without steering as control and three rabbits were used as blank control (without TMMC). Under fluoroscopic visualization, 0.027 lumen Progreat catheter was placed in the proper hepatic artery as far as possible from the right/left bifurcation. A Savvy (5 mm × 2 cm) balloon catheter (Cordis, Bridgewater, NJ) placed in the abdominal aorta at the level of the celiac trunk was inflated to reduce the blood flow velocity during TMMC injection. TMMC (40 mg) in saline solution (18 mL) were slowly injected (1.6 mL min^{-1}). Two hours after TMMC injection, the animal was euthanized with an i.v injection of sodium pentobarbital (120 mg kg^{-1}) (Vetoquinol, Lavaltrie, QC, Canada). The liver was carefully removed and stored in a 10% formalin solution (Chaptec, Pointe-aux-trembles, QC, Canada) at 4 °C. For the steering, a 1.5-T Siemens Avento clinical MRI scanner (Siemens, Erlangen, Germany) was used. The rabbit was placed in the center of two gradient coils equipped with a current reversal switch and a power supply (GMW Associates, San Carlos, CA) cooled down with a water cooler system (Opti Temp, Traverse City, MI). The magnetic gradient, generated by applying a 70-A current, depended on the distance between the two coils. Thus, depending of the size of the rabbit, a gradient of 288 ± 13-mT m^{-1} was applied. The liver was imaged before and after the TMMC injection with a coronal T2*-weighted gradient-echo sequence with the following parameters: relaxation time (TE) = 3.5 ms, repetition time (TR) = 225 ms, field of view (FOV) = 205 × 205 mm. To determine the steering efficiency, the TMMC and DOX doses were normalized by the weight of the sample analyzed. Complementary information is described in supplementary information section.

2.6. Histological analysis

Each lobe was carefully dissected and three 12-mm thick tissue slices located 4 mm apart were sectioned from each lobe. Liver tissues between each of these slices were used for DOX analysis. From each 12-mm section, a 4-mm thick slice of tissue was formalin fixed and paraffin-embedded. The remaining pieces were used for cobalt analysis. Each 4-mm thick slice was then cut with a microtome producing 4-μm sections which were subsequently layered on three slides. One slide was stained with hematoxylin and eosin (H&E) to confirm integrity of the liver parenchyma and one slide was stained with aniline blue to analyze TMMC distribution. Complementary information is described in supplementary information section.

2.7. Determination of cobalt levels in the liver

Each slice of each lobe (4 slices per lobe) was weighed (9.3 ± 2.0 g per lobe) and dried at 80 °C during 24 h. Then, the tissues were digested with a solution of HNO_3 (63 M) and HCl (36 M) at 80 °C. Cobalt concentration was measured with atomic absorption spectrometry (AAS) (S Series AAS, Fisher Thermo Scientific, Ottawa, ON, Canada). A blank control group was used to determine Co baseline.

2.8. Determination of DOX concentrations in vitro and in vivo

In vitro release and determination of DOX concentrations in liver and plasma are described in the supplementary information section.

2.9. Statistical analysis

In vitro steering results were compared with a student's *t*-test or an ANOVA test at 5% confidence (Sigma Plot software, Systat Software, Chicago, Il). *In vivo* steering data were compared with the Kruskal–Wallis one-way ANOVA with Dunn's post hoc analysis at 5% confidence. All values presented are expressed as mean ± standard deviation (s.d.).

3. Results and discussion

3.1. TMMC properties

FeCo nanoparticles (Fig. 2A) were synthesized and annealed to improve Ms (Table 1) [16]. The graphite shell surrounding the nanoparticle (Fig. 2A), maintained Ms during the encapsulation process. The required amount of FeCo nanoparticles was successfully co-encapsulated with DOX in TMMC (Table 1) having the appropriate diameter for liver chemoembolization (Fig. 2B and C). The loading of FeCo nanoparticles conferred to TMMC an Ms higher than that of iron oxide microparticles (60 emu g^{-1}) [18]. Following a burst release of 25% occurring within the first 5 min, the TMMC released DOX in a sustained fashion (Supplementary Fig. S1). After three days of elution, about 50% of the encapsulated DOX remained in TMMC. The release kinetics of TMMC was typical to that reported with other DOX-loaded PLGA microparticles [31]. TMMC were spherical in shape (Fig. 2B), an important feature to permit optimal arterial embolization [32], and steering in all directions relative to the MRI magnetic field [18]. Therefore, TMMC characteristics met all requirements for successful steering and chemoembolization.

3.2. In vitro steering

In vitro steering was performed in a phantom mimicking the hepatic artery and the right/left bifurcation circulated with real

Table 1
Characteristics of FeCo nanoparticles and TMMC used for *in vivo* MRN. Mean ± SD ($n = 6$).

FeCo nanoparticles	
Diameter (nm)	206 ± 62
Graphite layer thickness (nm)	10 ± 4
Atomic ratio Fe:Co (%)	59:41 ± 3:3
FeCo annealed Ms (emu g^{-1})	202 ± 6
FeCo prior to encapsulation Ms (emu g^{-1})	195 ± 10
TMMC	
Diameter (μm)	53 ± 19
Ms (emu g^{-1})	72 ± 3
FeCo nanoparticle loading (%, *w*/*w*)	37 ± 2.7
Doxorubicin loading (%, *w*/*w*)	3.2 ± 0.5

flow velocities (Supplementary Fig. S3). Steering efficiency was defined as the reduction of the TMMC (or drug) dose in the untargeted area in the presence of magnetic steering *versus* the negative control (no steering). The effect of four experimental parameters on the steering efficiency was examined: (i) magnetic gradient magnitude, (ii) TMMC steering properties (Ms and diameter), (iii) the distance between the catheter tip and the bifurcation (Fig. 1) and (iv) flow velocity. The last two parameters are critical for clinical application of MRN since catheter position in the artery and flow velocity might change from one subject to the other. Flow velocity is also influenced by the treatment procedure and decreases upon liver embolization [33].

Fig. 3 shows that in all experimental settings, MRN allowed a reduction of embolization in the non targeted area (steering efficiency $> 0\%$). According to Fig. 3A, steering efficiency with high flow velocity decreased significantly from 60 to 44% when the gradient decreased from 400 to 200-mT m^{-1}. Hence, the highest gradient should be used for an efficient MRN. The impact of TMMC diameter (and corresponding Ms) on steering efficiency was assessed in Fig. 3B. Increasing the TMMC diameter from 30 ($Ms = 49$ emu g^{-1}) to 53 μm ($Ms = 72$ emu g^{-1}) improved the steering efficiency. In clinical practice, particle diameter below 30 μm could entail the risk of extravasation and lung embolization [32]. According to the steering model shown in Supplementary Fig. S2, TMMC with diameters greater than 50 μm could further improve the MRN efficiency [16]. However, the chemoembolization with larger particles could also lead to a less distal distribution resulting in a lower dose of DOX delivered to tumor.

On Fig. 3C, it can be seen that the flow velocity had a major impact on the steering efficiency. It increased from 19 to 67% when the flow velocity decreased from 12 to 7.5 cm s^{-1} (case where the catheter tip was positioned 20 mm from the bifurcation). The reduction of the flow velocity during the experiment (as is expected to occur upon the TMMC injection) led to a steering efficiency of 35%. When the catheter was placed at 33 mm from the bifurcation, no significant difference in efficiency was observed between the three flow velocities (Fig. 3C, last 3 columns). Accordingly, the impact of the flow velocity on steering efficiency was greater when the catheter tip was located close to the bifurcation and was negligible away from it. At moderate flow velocity, the impact of catheter position on efficiency was minimal.

Based on these results and in order to maximize *in vivo* steering efficiency, the catheter should be placed as far away as practically possible from the bifurcation, the flow velocity reduced to its minimum and the highest gradient magnitude applied. In the optimal conditions, the steering efficiency reached 76%, suggesting a real potential of MRN to minimize chemoembolization of the untargeted area.

3.3. *In vivo* steering

In vivo steering efficiency was studied by measuring TMMC and DOX distribution into the right and left lobes according to four methods: (i) magnetic resonance (MR) images of the liver (Fig. 4A), (ii) histology analysis (Fig. 4B, Fig. S4A), (iii) assay of DOX (Fig. S4B) and (iv) Co (Fig. 4C) levels. The distribution ratio between the right and left lobe was compared in the presence and absence of steering. On the T2*-weighted MR images (Fig. 4A), TMMC appeared as dark pixels because of the signal loss due to magnetic field inhomogeneity induced by the high TMMC magnetization [34,35]. After the steering to the left liver bifurcation (Fig. 4A), TMMC were mainly localized to the left lobes and the right lobe appeared to be free from TMMC. This qualitative result illustrates the attractive potential of MRN to target a specific area. It also shows that TMMC can be tracked *in situ*, an interesting feature for clinicians. Interventional radiologists will be able to monitor the chemoembolization progress and efficiency. In comparison, the DEB presently used in the clinic are not visible on any imaging modality. They are injected with a contrast agent under fluoroscopic guidance [29].

The histological images (Fig. 4B), confirmed that TMMC successfully embolized into the distal branches of the hepatic artery. No TMMC were detected in the liver parenchyma outside the vascular network. According to TMMC and DOX distribution

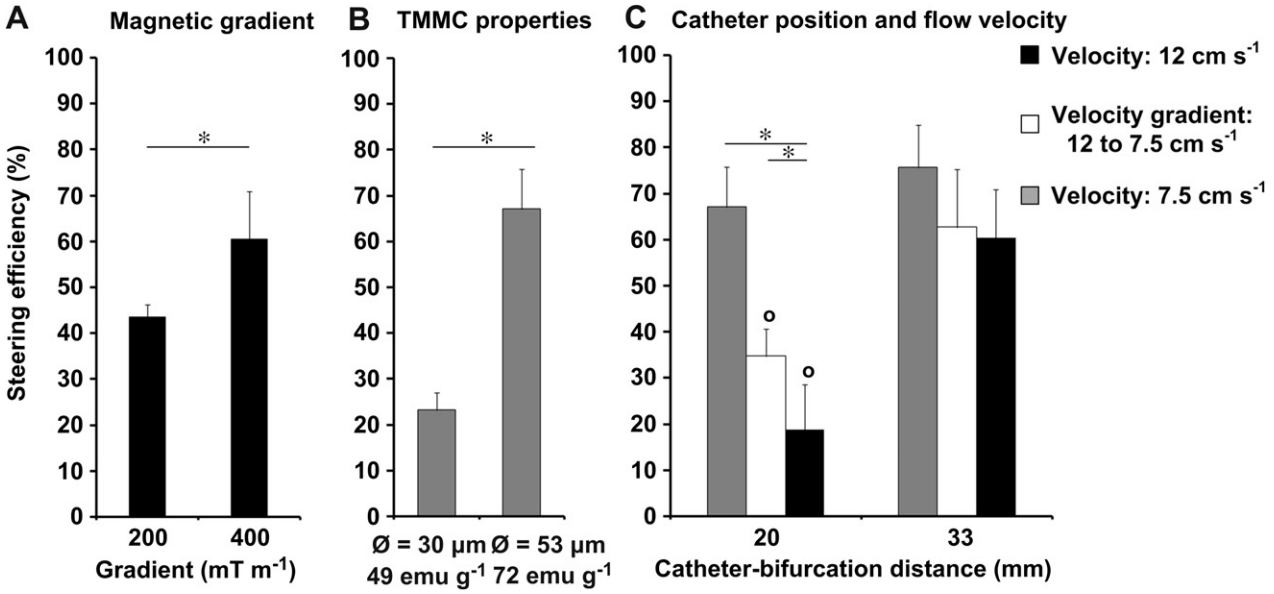

Fig. 3. *In vitro* TMMC steering efficiency as a function of the magnetic gradient (A), TMMC steering properties (B), flow velocity and the distance between catheter tip and right/left hepatic artery bifurcation (C). In (A) and (C), TMMC with $Ms = 72 \pm 3$ emu g^{-1} and $Ø = 53 \pm 19$ μm were used. On (B) and (C), a gradient of +/− 400-mT m^{-1} was applied. On (A) and (B) the flow was set at 12 and at 7.5 cm s^{-1}, respectively. On (C) a velocity gradient (from 12 to 7.5 cm s^{-1}) was applied to mimic the flow velocity decrease due to the embolization. On (A) and (B) the catheter tip was placed at 33 and 20 mm, respectively. *$p < 0.05$ between the groups, 0 $p < 0.05$ between the groups catheter-bifurcation = 20 mm and catheter-bifurcation = 33 mm. Mean ± SD ($n = 3$).

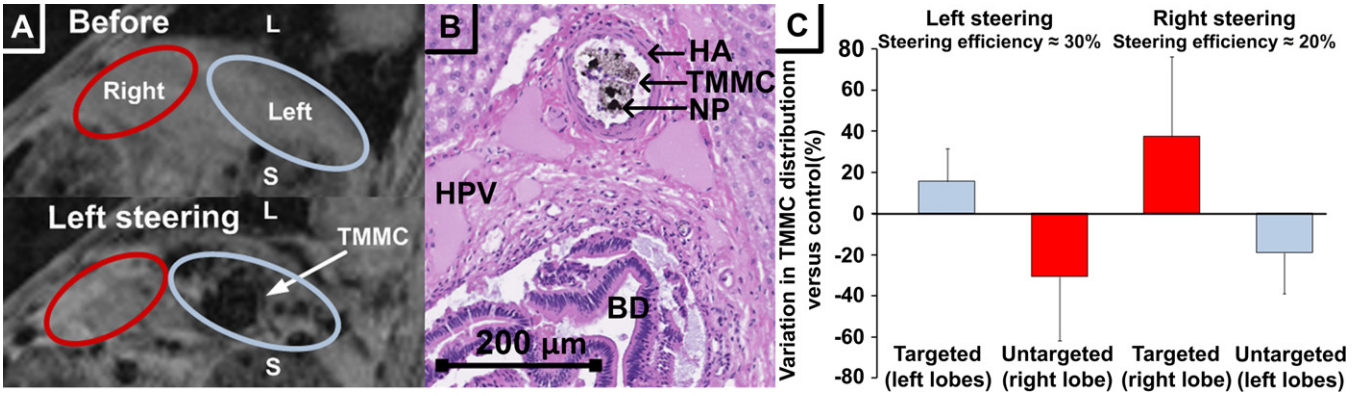

Fig. 4. *In vivo* TMMC steering data. Images A represent T2*-weighted MR images of the rabbit liver before and after TMMC left steering. The red line delineates the right lobe and the blue line shows the left lobes. S indicates the stomach and L the lungs. Image B displays a microscopic view of the liver parenchyma and the blood vessels stained with hematoxylin and eosin (HA = branch of hepatic artery; HPV = hepatic portal vein; BD = bile duct; NP = FeCo nanoparticles). TMMC are located within a branch of the hepatic artery. Image C shows the variation in TMMC distribution *versus* control in the liver lobes with left and right steering based on Co analysis. Significant difference ($p = 0.029$) between the steering group ($n = 4$) *versus* the control group ($n = 3$) was obtained. Mean ± SD.

analyses (Fig. 4C and Supplementary Fig. S4), MRN significantly controlled the distribution of these therapeutic particles as compared to the control. The same distribution profile into each lobe was obtained for the three analyses, with a correlation coefficient (r) > 0.98 between the methods. The steering to the right or left bifurcation led to an increase in the TMMC deposition in the targeted lobe (Fig. 4C). More importantly, a decrease in the TMMC levels in the untargeted lobe was obtained. Regarding the plasmatic DOX concentrations, after a burst effect at 5 min, the drug concentration in the systemic circulation rapidly decreased to very low levels (Supplementary Fig. S5). The *in vivo* burst effect correlated well with that observed *in vitro* (Supplementary Fig. S1). Moreover, the pharmacokinetic profile resembled that reported for DEB [28].

To the best of our knowledge, this is the first study showing that steering can be achieved in the hepatic artery located at a depth of 4 cm below the skin with moderate blood flow with an MRI scanner. Steering efficiency was higher with the left steering compared to the right steering (Fig. 4C and Supplementary Fig. S4). Hence, MRN was more efficient to preserve right liver lobe from the chemoembolization than left lobes. Furthermore, the right lobe targeting was better. As only one third of the TMMC dose reached the right lobe without steering because of the natural difference in blood supply between the lobes according to their weight (right lobe = 22 ± 3 g and left lobes = 33 ± 2 g), the effects of MRN were more important in the right lobe.

Variation in the steering efficiency was observed from one animal to another. This variation could be mainly attributed to the catheter tip position and the blood flow velocity (Fig. 1 and Fig. 3C). In fact, the catheter position was limited by anatomical constraints and it was generally placed at 20 ± 2 mm from the right/left bifurcation (Fig. 1). At this distance, according to the *in vitro* results (Fig. 3C), the efficiency is significantly affected by the flow velocity. We supposed that the variation of blood flow velocity between each animal could account for the observed variability. In one experiment, where the catheter tip was placed at a distance greater than 30 mm, the steering efficiency increased to 50%. This result was in good agreement with the *in vitro* steering data (Fig. 3C).

The *in vivo* steering efficiency could in principle be improved by the following measures (Fig. 3): (i) measuring blood flow prior to MRN and reducing it to an adequate value with a balloon catheter, (ii) embolizing the gastroduodenal artery to place the catheter as far away as possible from the bifurcation, and (iii) increasing the magnetic gradient to 400-mT m^{-1}. In a clinical setting, TMMC could be injected through an implantable arterial catheter positioned in the main hepatic artery equipped with a balloon on its extremity. With this design, it could be possible to perform alternative embolization of the right and left lobe or hyperselective embolization without the need for repetitive catheterization.

4. Conclusion

New therapeutic particles for MRI targeting were successfully developed and validated *in vivo* taking into consideration MRN and liver chemoembolization constraints. These particles possessed a very attractive combination of properties: MRN compatibility, MRI tracking property, appropriate diameter for the embolization of hepatic artery branches, and sustained drug release. MRN was successfully carried out *in vitro* and *in vivo*. MRN in the hepatic artery of these particles to control their distribution in the liver represents a significant step toward the development of tumor targeted therapies and better control over the side effects. This strategy could improve the therapeutic outcome of chemoembolization in patients with poor prognostic outlook. Further work will aim to target a liver tumor to evaluate MRN therapeutic efficacy. In addition, MRN in a vascular network with several bifurcations will be investigated for hyperselective embolization.

Acknowledgments

This project was supported by the Canadian Institutes for Health Research (CIHR), the Canada Research Chair program, the Canada Foundation for Innovation (CFI), the Natural Sciences and Engineering Research Council of Canada (NSERC), and Fonds Québécois de la Recherche sur la Nature et les Technologies (FQRNT). GS. was supported by a clinical research scholarship from Fonds de la recherche en santé du Québec (FRSQ) The authors acknowledge Julie Hinsinger (UdM) and the histological team (UdM) for their work on the liver preparation, Hélène Héon (CHUM), the animal house care team (CHUM), Jocelyne Lavoie (CHUM), Gilles Beaudoin (CHUM), Gael Bringout (EPM), Charles Tremblay (EPM) and the students from the NanoRobotics laboratory at EPM for their help during *in vivo* tests.

Appendix

Figures with essential color discrimination. Figs. 1,2 and 4 in this article are difficult to interpret in black and white. The full color

images can be found in the online version, at doi:10.1016/j.biomaterials.2010.12.059

Appendix. Supplementary data

Supplementary data associated with this article can be found, in the online version, at doi:10.1016/j.biomaterials.2010.12.059.

References

[1] Widder KJ, Morris RM, Poore G, Howard Jr DP, Senyei AE. Tumor remission in Yoshida sarcoma-bearing rats by selective targeting of magnetic albumin microspheres containing doxorubicin. Proc Natl Acad Sci USA 1981;78:579–81.

[2] Dames P, Gleich B, Flemmer A, Hajek K, Seidl N, Wiekhorst F, et al. Targeted delivery of magnetic aerosol droplets to the lung. Nat Nanotechnol 2007;2:495–9.

[3] Amirfazli A. Nanomedicine: magnetic nanoparticles hit the target. Nat Nanotechnol 2007;2:467–8.

[4] Dobson J. Cancer therapy: a twist on tumour targeting. Nat Mater 2010; 9:95–6.

[5] Sun C, Lee JS, Zhang M. Magnetic nanoparticles in MR imaging and drug delivery. Adv Drug Deliv Rev 2008;60:1252–65.

[6] Liu HL, Hua MY, Yang HW, Huang CY, Chu PC, Wu JS, et al. Magnetic resonance monitoring of focused ultrasound/magnetic nanoparticle targeting delivery of therapeutic agents to the brain. Proc Natl Acad Sci USA 2010;107:15205–10.

[7] Chertok B, David AE, Yang VC. Polyethyleneimine-modified iron oxide nanoparticles for brain tumor drug delivery using magnetic targeting and intracarotid administration. Biomaterials 2010;31:6317–24.

[8] Wilson MW, Kerlan Jr RK, Fidelman NA, Venook AP, LaBerge JM, Koda J, et al. Hepatocellular carcinoma: regional therapy with a magnetic targeted carrier bound to doxorubicin in a dual MR imaging/ conventional angiography suite–initial experience with four patients. Radiology 2004;230:287–93.

[9] Kobeiter H, Georgiades CS, Leakakos T, Torbenson M, Hong K, Geschwind JF. Targeted transarterial therapy of Vx-2 rabbit liver tumor with Yttrium-90 labeled ferromagnetic particles using an external magnetic field. Anticancer Res 2007;27:755–60.

[10] Namiki Y, Namiki T, Yoshida H, Ishii Y, Tsubota A, Koido S, et al. A novel magnetic crystal-lipid nanostructure for magnetically guided in vivo gene delivery. Nat Nanotechnol 2009;4:598–606.

[11] Shi J, Votruba AR, Farokhzad OC, Langer R. Nanotechnology in drug delivery and tissue engineering: from discovery to applications. Nano Lett 2010;10: 3223–30.

[12] Polyak B, Fishbein I, Chorny M, Alferiev I, Williams D, Yellen B, et al. High field gradient targeting of magnetic nanoparticle-loaded endothelial cells to the surfaces of steel stents. Proc Natl Acad Sci USA 2008;105:698–703.

[13] Chorny M, Fishbein I, Yellen BB, Alferiev IS, Bakay M, Ganta S, et al. Targeting stents with local delivery of paclitaxel-loaded magnetic nanoparticles using uniform fields. Proc Natl Acad Sci USA 2010;107:8346–51.

[14] Plank C. Nanomedicine: silence the target. Nat Nanotechnol 2009;4:544–5.

[15] Martel S, Mathieu JB, Felfoul O, Chanu A, Aboussouan E, Tamaz S, et al. Automatic navigation of an untethered device in the artery of a living animal using a conventional clinical magnetic resonance imaging system. Appl Phys Lett 2007;90:114105–11.

[16] Pouponneau P, Leroux JC, Martel S. Magnetic nanoparticles encapsulated into biodegradable microparticles steered with an upgraded magnetic resonance imaging system for tumor chemoembolization. Biomaterials 2009;30:6327–32.

[17] Pouponneau P, Savadogo O, Napporn T, Yahia L, Martel S. Corrosion study of iron-cobalt alloys for MRI-based propulsion embedded in untethered microdevices operating in the vascular network. J Biomed Mater Res B Appl Biomater 2010;93:203–11.

[18] Mathieu JB, Martel S. Steering of aggregating magnetic microparticles using propulsion gradients coils in an MRI Scanner. Magn Reson Med 2010;63: 1336–45.

[19] Mathieu JB, Martel S. Magnetic microparticle steering within the constraints of an MRI system: proof of concept of a novel targeting approach. Biomed Microdevices 2007;9:801–8.

[20] Riegler J, Wells JA, Kyrtatos PG, Price AN, Pankhurst QA, Lythgoe MF. Targeted magnetic delivery and tracking of cells using a magnetic resonance imaging system. Biomaterials 2010;31:5366–71.

[21] Bruix J, Llovet JM. Major achievements in hepatocellular carcinoma. Lancet 2009;373:614–6.

[22] Cabibbo G, Latteri F, Antonucci M, Craxi A. Multimodal approaches to the treatment of hepatocellular carcinoma. Nat Clin Pract Gastroenterol Hepatol 2009;6:159–69.

[23] Lo CM, Ngan H, Tso WK, Liu CL, Lam CM, Poon RT, et al. Randomized controlled trial of transarterial lipiodol chemoembolization for unresectable hepatocellular carcinoma. Hepatology 2002;35:1164–71.

[24] Liapi E, Geschwind JF. Transcatheter and ablative therapeutic approaches for solid malignancies. J Clin Oncol 2007;25:978–86.

[25] Kennedy AS, Kleinstreuer C, Basciano CA, Dezarn WA. Computer modeling of yttrium-90-microsphere transport in the hepatic arterial tree to improve clinical outcomes. Int J Radiat Oncol Biol Phys 2010;76:631–7.

[26] Liapi E, Geschwind JF. Chemoembolization for primary and metastatic liver cancer. Cancer J 2010;16:156–62.

[27] Varela M, Real MI, Burrel M, Forner A, Sala M, Brunet M, et al. Chemoembolization of hepatocellular carcinoma with drug eluting beads: efficacy and doxorubicin pharmacokinetics. J Hepatol 2007;46:474–81.

[28] Hong K, Khwaja A, Liapi E, Torbenson MS, Georgiades CS, Geschwind JF. New intra-arterial drug delivery system for the treatment of liver cancer: preclinical assessment in a rabbit model of liver cancer. Clin Cancer Res 2006;12:2563–7.

[29] Reyes DK, Vossen JA, Kamel IR, Azad NS, Wahlin TA, Torbenson MS, et al. Single-center phase II trial of transarterial chemoembolization with drug-eluting beads for patients with unresectable hepatocellular carcinoma: initial experience in the United States. Cancer J 2009;15:526–32.

[30] Seo WS, Lee JH, Sun X, Suzuki Y, Mann D, Liu Z, et al. FeCo/graphitic-shell nanocrystals as advanced magnetic-resonance-imaging and near-infrared agents. Nat Mater 2006;5:971–6.

[31] Lin R, Shi Ng L, Wang CH. In vitro study of anticancer drug doxorubicin in PLGA-based microparticles. Biomaterials 2005;26:4476–85.

[32] Hong K, Kobeiter H, Georgiades CS, Torbenson MS, Geschwind JF. Effects of the type of embolization particles on carboplatin concentration in liver tumors after transcatheter arterial chemoembolization in a rabbit model of liver cancer. J Vasc Interv Radiol 2005;16:1711–7.

[33] Lopez-Benitez R, Richter GM, Kauczor HU, Stampfl S, Kladeck J, Radeleff BA, et al. Analysis of nontarget embolization mechanisms during embolization and chemoembolization procedures. Cardiovasc Intervent Radiol 2009;32: 615–22.

[34] Shapiro EM, Skrtic S, Sharer K, Hill JM, Dunbar CE, Koretsky AP. MRI detection of single particles for cellular imaging. Proc Natl Acad Sci USA 2004;101: 10901–6.

[35] Gupta T, Virmani S, Neidt TM, Szolc-Kowalska B, Sato KT, Ryu RK, et al. MR tracking of iron-labeled glass radioembolization microspheres during transcatheter delivery to rabbit VX2 liver tumors: feasibility study. Radiology 2008;249:845–54.